

Sparse or Dense? A Mechanistic Estimation of Computation Density in Transformer-based LLMs

Corentin Kervadec¹ Iuliia Lysova¹ Marco Baroni^{1,2} Gemma Boleda^{1,2}

Abstract

Transformer-based large language models (LLMs) are comprised of billions of parameters arranged in deep and wide computational graphs. Several studies on LLM efficiency optimization argue that it is possible to prune a significant portion of the parameters, while only marginally impacting performance. This suggests that the computation is not uniformly distributed across the parameters. We introduce here a technique to systematically quantify computation density in LLMs. In particular, we design a density estimator drawing on mechanistic interpretability. We experimentally test our estimator and find that: (1) contrary to what has been often assumed, LLM processing generally involves dense computation; (2) computation density is dynamic, in the sense that models shift between sparse and dense processing regimes depending on the input; (3) per-input density is significantly correlated across LLMs, suggesting that the same inputs trigger either low or high density. Investigating the factors influencing density, we observe that predicting rarer tokens requires higher density, and increasing context length often decreases the density. We believe that our computation density estimator will contribute to a better understanding of the processing at work in LLMs, challenging their symbolic interpretation.

1. Introduction

Modern transformer-based LLMs are composed of billions of weights arranged in a very large computational graph. While inference nominally executes the full model for every input, it remains unclear whether the effective amount of computation required to generate a prediction is close to

¹Department of Translation and Language Sciences, Universitat Pompeu Fabra, Barcelona, Spain ²Catalan Institute of Research and Advanced Studies (ICREA), Barcelona, Spain. Correspondence to: Corentin Kervadec <corentin.kervadec@gmail.com>.

Preprint. February 2, 2026.

The dozen or so people who had worked so hard stood in a circle congratulating each other.

“That was a good day,” one of them said.

“I’m so proud of all of you,” another said

Figure 1. For each token generated by the LLM (here: Mistral-7B (Jiang et al., 2024a)), we measure the computation density of the trace, indicating the amount of computation required to process the input and output a prediction. Each token is colored according to its density, ranging from low (cold color) to high (warm).

the full-model power or it is considerably sparser, as well as the extent to which this effective amount of computation is dependent on specific input properties. Answering these questions has both practical and theoretical implications. From a practical point of view, precisely quantifying the true sparsity of LLM computation and predicting which inputs require more computation can help building more efficient models through pruning, distillation or other techniques. Establishing sparsity is also a prerequisite for meaningful application of interpretability techniques such as circuit analysis, that assume that many language/knowledge processes in LLMs can be reduced to the mechanics of a sparse sub-graph (Ferrando et al., 2024a; Cammarata et al., 2020; Ameisen et al., 2025). From a theoretical point of view, our pursue bears on two fundamental questions in cognitive science. On the one hand, language competence has traditionally being modeled as a sparse, symbolic, rule-based system greatly at odds with LLMs’ highly distributed nature (Smolensky et al., 2022). If LLMs turned out to rely on much sparser circuits during average processing, this would pave the way for a reconciliation between the symbolic and distributed views of language (Boleda, 2025). On the other hand, the nature of linguistic complexity and how to measure it are fundamental topics in linguistics (e.g., Jackendoff & Wittenberg, 2014). If we found that the amount of effective computation in LLMs depended on specific properties of their inputs, this would suggest that LLMs are useful for this line of inquiry.

In this paper, we want to characterize computation density as a way to better understand LLM language processing.

To this end, we propose a way to calculate the amount of effective computation performed by an LLM in response to an input. Our method, based on automated circuit discovery (Ferrando & Voita, 2024), given an input, quantifies the number of computational graph edges that must be recruited to ensure that the LLM produces output that is equivalent, up to an error threshold, to the output generated by a pass through the full graph. We refer to this quantity as the *trace size*. Varying the threshold allows for a systematic examination of the performance/complexity trade-off in LLMs, leading to our measure of *computation density* (Fig. 1).

We analyze 13 different LLMs and find that, on average, the trace size needed to preserve unaltered performance constitutes a large proportion of the full graph size. Thus, we do not find evidence for pervasive sparse computation in LLMs. At the same time, we find substantial input-dependent variance in density, suggesting that LLMs do recruit more or less resources based on the nature of the input. Strikingly, different LLMs show very similar density distributions across inputs, suggesting that resource allocation depends on intrinsic properties of linguistic inputs, rather than on the architectural details of specific models. More specifically, three results suggest that density is indeed related to the complexity of the input: 1) the density distribution is positively correlated with LLM output entropy (LLMs' own uncertainty estimate); 2) density increases for rarer words (which are harder to guess than more frequent words); 3) density decreases as context grows, that is, as the LLM has more information as to what is being said.¹

2. Background

Sparsity in LLMs Our work is tightly related to the notion of sparsity in LLMs and neural networks in general. Studying the sparsity of neural networks is well-established, dating back to early work (LeCun et al., 1989). In the context of deep learning, the Lottery Ticket Hypothesis (Frankle & Carbin, 2019) posits that dense, randomly initialized networks contain sparse sub-networks (“winning tickets”) that can match the performance of the full model when trained in isolation. This sparsity seems to still hold true for LLMs. For instance, Voita et al. (2023) observed that ReLU-based LLMs contain a large proportion of “dead” neurons, particularly in the early layers, that are always inactive.

Based on the hypothesis that actual LLM computation is sparse, a large body of work proposed various methods to optimally prune LLM parameters. Unstructured pruning operates at the neuron or weight level (Luo et al., 2024; Sun et al., 2023). Structural pruning targets coherent components, such as attention heads (Michel et al., 2019) or

¹The code and data required to reproduce the experiments will be made publicly available on a Github repository upon acceptance.

entire layers (Li et al., 2024). With these methods, Lad et al. (2024) observed that middle layers are remarkably robust to deletion (implying low computation density), while early and late layers remain critical.

While static pruning identifies permanently redundant parameters, a growing body of evidence suggests that computation density is dynamic, shifting significantly depending on the input instance. For instance, Liu et al. (2023) estimate that over 80% of attention heads and 95% of MLP neurons can be dynamically pruned during inference with minimal degradation. Bansal et al. (2023) extract task-based sub-network experts from a trained LLM. Other efficiency methods exploit this sparsity by skipping computation on the fly. For example, Zhang et al. (2022) demonstrates that Feed-Forward layers can be decomposed into modular “experts,” with only a fraction of them needed for any given input. Similarly, D-LLM (Jiang et al., 2024b) or Deja Vu (Liu et al., 2023) introduce token-adaptive strategies, dynamically skipping units for dispensable tokens. Using a similar approach, Lee et al. (2024) reached a sparsity of 50% on downstream tasks with little loss of accuracy. Furthermore, recent studies suggest that this dynamic sparsity is correlated with the intrinsic difficulty or “complexity” of the input. Thus, Fan et al. (2024) observed that not all layers of LLMs are necessary during inference, and that simpler tasks require fewer layers, while more complex tasks require more layers of inference. Finally, Lee et al. (2025) provides a different view on sparsity and introduce the concept of intrinsic “token complexity,” finding that difficult reasoning tasks impose a hard floor on the number of generated tokens (and thus computational volume) required for success.

We have a different purpose with respect to this work: rather than proposing task-specific pruning strategies, we seek a general measure that quantifies the amount of effective processing performed by a LLM in response to an input. We consequently will measure trace size with respect to the ability of a sub-graph to reproduce the full output distribution during generic next-token prediction, rather than based on some discretized measure of task success.

Mechanistic Interpretability To rigorously quantify density in LLMs, we leverage methods from mechanistic interpretability. This line of research generally views LLMs not as black boxes, but as computational graphs composed of discrete, human-interpretable “circuits” (Olah et al., 2018; Cammarata et al., 2020; Ameisen et al., 2025). Notable examples include the discovery of circuits responsible for the greater-than operation (Hanna et al., 2023), Indirect Object Identification (Wang et al., 2022), subject-verb agreement (Ferrando et al., 2024a), and knowledge retrieval (Meng et al., 2022). Circuit discovery can be automated, for instance using greedy search (Conmy et al., 2023), sparse dictionary learning (Bricken et al., 2023), acti-

vation patching (Syed et al., 2024), or gradient-based pruning (Bhaskar et al., 2024). Despite notable achievements, circuit discovery faces limitations. The circuits often apply only to a narrow range of specific processing operations and frequently fail to generalize robustly across the full diversity of sentences or models (Méloux et al., 2025; Sharkey et al., 2025), highlighting the importance of measuring their faithfulness (Hanna et al., 2024).

We rely here on an automated circuit discovery technique, namely the Information Flow Route (IFR) method (Ferrando & Voita, 2024), which leverages attribution to efficiently identify circuits at scale. However, rather than applying it to the identification of task-specific circuits, we repurpose it as a general method to estimate the smallest sub-graphs reaching different degrees of reconstruction success.

3. Methodology

3.1. LLM as a Computational Graph

Our work is grounded in the formal representation of a language model’s internal processes as a computational graph (Ferrando & Voita, 2024). We consider a language model, M , that accepts an input sequence of n tokens, $\mathbf{t} = (t_1, \dots, t_n)$, and computes a probability distribution over the next token, $P(t_{n+1}|\mathbf{t})$. This process is modeled as a forward pass through a directed acyclic graph $G = (V, E)$; nodes V represent intermediate states and edges E represent computational operations transforming information flow.

We focus on the transformer architecture (Vaswani et al., 2017), the standard for modern LLMs. Following the decomposition by Elhage et al. (2021), the forward pass consists of a sequence of residual blocks. First, discrete tokens are embedded into continuous vector representations, $\mathbf{h}^0 = (h_1^0, \dots, h_n^0)$, forming the initial nodes of the graph. These representations are iteratively transformed through L layers. The state at layer l , denoted $\mathbf{h}^l = (h_1^l, \dots, h_n^l)$, is a function of the previous layer’s activations.

Each layer l is a residual block composed of two primary sub-layers: Multi-Head Attention (MHA) and a Multi-Layer Perceptron (MLP). Crucially, the residual connection allows us to express the update as an additive sum. For a specific token i at layer l , the update rules are:

$$\bar{h}_i^{l+1} = h_i^l + \sum_{k=1}^{N_H} \sum_{j=1}^n \phi^{l,k}(h_i^l, h_j^l) \quad (1)$$

$$h_i^{l+1} = \bar{h}_i^{l+1} + \text{MLP}_l(\bar{h}_i^{l+1}) \quad (2)$$

where N_H is the number of attention heads. In Eq. (1), $\phi^{l,k}(h_i^l, h_j^l)$ represents the *attention head contribution*: the vector “moved” from source token j to target token i by head k (see Ferrando & Voita, 2024, for more details). This pairwise decomposition is central to our graph formulation.

The computational graph G is defined as follows: **Nodes** (V): The set of all intermediate token representations $\{h_i^l \mid l \in [0, L], i \in [1, n]\}$; **Edges** (E): The transformations connecting these representations.

By unrolling Equations 1 and 2, we observe that the vector representation at any node is simply the sum of vectors from its incoming edges. This yields a granular view of information flow. Formally, an MHA sub-layer is decomposed into $N_H \times n + 1$ edges per target token, as follows:

$$\bar{h}_i^{l+1} = \underbrace{h_i^l}_{\text{Residual Edge}} + \sum_{k,j} \underbrace{\phi^{l,k}(h_i^l, h_j^l)}_{\text{Attention Edges}} \quad (3)$$

An MLP sub-layer gives rise to 2 edges per target token:

$$h_i^{l+1} = \underbrace{\bar{h}_i^{l+1}}_{\text{Residual Edge}} + \underbrace{\text{MLP}_l(\bar{h}_i^{l+1})}_{\text{MLP Edge}} \quad (4)$$

It is important to note that both nodes *and edges* are defined token-wise. This allows for a finer modeling of information routing compared to approaches that aggregate head outputs into a single edge per target token (e.g., Syed et al., 2024).

3.2. Trace Definition and Faithfulness

We define a *Trace*, T , as a computational subgraph of the full model G . Formally, $T = (V_T, E_T)$ where $V_T \subseteq V$ and $E_T \subseteq E$. In practice, the trace is realized by applying a binary mask, $M = \{m_e\}_{e \in E}$, to the computational graph, where $m_e = 1$ if edge $e \in E_T$ and 0 otherwise. For example, the masked update rule for the MHA sub-layer (previously Eq. 3) becomes:

$$\bar{h}_i^{l+1} = m_{i,\text{res}}^l \cdot h_i^l + \sum_{k,j} m_{i,j}^{l,k} \cdot \phi^{l,k}(h_i^l, h_j^l) \quad (5)$$

where $m \in \{0, 1\}$ are the binary decisions for the residual and attention edges respectively.

We will analyze the *density* of computation, relating the size of the trace to its predictive fidelity. The size, s , is defined as the sparsity ratio $s = |E_T|/|E_G| \in [0, 1]$. We denote by $T[s]$ a trace containing a fraction s of the total edges.

TV distance To evaluate the quality of a trace, we measure its *faithfulness*: how well the masked model output P_T approximates the full model output P_G . Unlike prior work that often focuses on binary task success (e.g., whether the correct token is the top-1 prediction), we adopt a more conservative and general approach by measuring the preservation of the full output distribution. We quantify this using the Total Variation (TV) distance:

$$\delta_{TV}(P_G, P_T) = \frac{1}{2} \sum_{v \in \mathcal{V}} |P_G(v) - P_T(v)| \quad (6)$$

where \mathcal{V} is the token vocabulary. A low δ_{TV} indicates that the trace is *sufficient* to recover the model’s behavior. However, sufficiency does not imply *necessity*. To assess necessity—whether the edges in T are the *only* ones capable of producing the output—we employ a complementary evaluation (detailed in App. C.2), where we ablate *only* the trace edges and observe the degradation.

We select TV distance over alternatives such as the Kullback-Leibler (KL) divergence for two reasons. First, KL divergence is unbounded and sensitive to relative errors, meaning it can be dominated by discrepancies in the low-probability tail. In contrast, TV distance measures the absolute difference in probability mass. This ensures our metric focuses on the dominant modes of the distribution—where the model’s actual predictions lie—rather than being disproportionately affected by the noisy tail. Second, TV provides a bounded metric $\in [0, 1]$, ensuring the stability of the density integral ρ defined in the subsequent section.

3.3. Trace Extraction via Information Flow Routes

The challenge of trace extraction is to identify the subset of edges $E_T \subset E_G$ that are *sufficient* to reconstruct the model’s output distribution. Given the scale of the models analyzed (1B to 13B parameters), computationally expensive methods like causal interventions or activation patching are infeasible for identifying all edges. Thus, we opt for a training-free, activation-based strategy that requires only a single pass.

Magnitude-based Importance Score We adapt the Information Flow Route (IFR) framework (Ferrando & Voita, 2024) to our graph formulation. This approach filters edges based on an importance score. While the original implementation utilized a similarity-based metric (comparing node vs. edge embeddings), we observe that this metric correlates poorly with the distributional faithfulness required for our study. Instead, we opt for a vanilla magnitude-based importance score, positing that the impact of an operation is proportional to the magnitude of its update vector. For any edge e carrying a vector \mathbf{v}_e (e.g., an attention head output $\phi^{l,k}$), we define its importance $\mathcal{I}(e)$ as the L1 norm:

$$\mathcal{I}(e) = \|\mathbf{v}_e\|_1 \quad (7)$$

Recursive Graph Traversal To construct the trace T , we perform a recursive backward search on the computational graph G , starting from the final output node h_n^L . This is a lightweight graph traversal that does not require gradient computation. The algorithm proceeds as follows: for a current node in the trace, we examine its incoming edges. An edge e and its source node are added to the trace if and only if the importance score exceeds a threshold τ :

$$E_T(\tau) = \{e \in E_G \mid e \text{ is connected to } T \text{ and } \mathcal{I}(e) \geq \tau\} \quad (8)$$

The threshold τ serves as a control parameter for the trace size, allowing us to sweep from sparse, highly selective traces to the full dense graph.

3.4. Estimating Computational Density

We quantify the global sparsity of the model using a scalar metric, the *Computational Density*, denoted ρ . We define ρ as the Area Under the Curve (AUC) of the reconstruction error plotted against the trace size:

$$\rho = \int_0^1 \epsilon(s) ds \quad (9)$$

where $\epsilon(s) = \delta_{TV}(P_G, P_{T[s]})$ is the faithfulness error for a trace of size s . Intuitively, ρ measures the model’s resistance to pruning: **Low ρ (Sparse):** The error $\epsilon(s)$ drops rapidly to zero even for small s , implying that a few edges suffice to replicate the computation; **High ρ (Dense):** The error remains significant until s approaches 1, implying that information is distributed diffusely across the graph.

Discrete Estimation In practice, computing the continuous integral is intractable. We estimate ρ by evaluating the error at a finite set of discrete trace sizes $S = \{s_0, s_1, \dots, s_K\}$, where $0 = s_0 < s_1 < \dots < s_K = 1$. The density $\hat{\rho}$ is computed using the trapezoidal rule:

$$\hat{\rho} \approx \frac{1}{2} \sum_{k=1}^K (s_k - s_{k-1}) \cdot [\epsilon(s_k) + \epsilon(s_{k-1})] \quad (10)$$

To maintain computational efficiency while capturing fine-grained behavior, we use a list of fixed thresholds.

4. How Dense is the Computation in LLMs?

We report two main experiments. The first (this section) aims at measuring the typical density of LLM computation. The second (next section) focuses on input characteristics that might determine the density.

4.1. Method

We use a dataset of 5000 fragments from Wikitext (Merity et al., 2017). These fragments were selected to contain 20 words on average (one or two sentences), making sure that they start with a beginning of sentence and end with a full word or punctuation (no word fragment).

For each input, we extract the trace at 15 levels of granularity, spanning from very sparse to very dense, using an empirically determined grid of thresholds τ (App. B). A small τ leads to larger traces, while a larger τ leads to smaller traces. As explained above, the threshold serves as an *importance filter*, excluding edges in the computational graph that are below it. At each threshold, we measure the

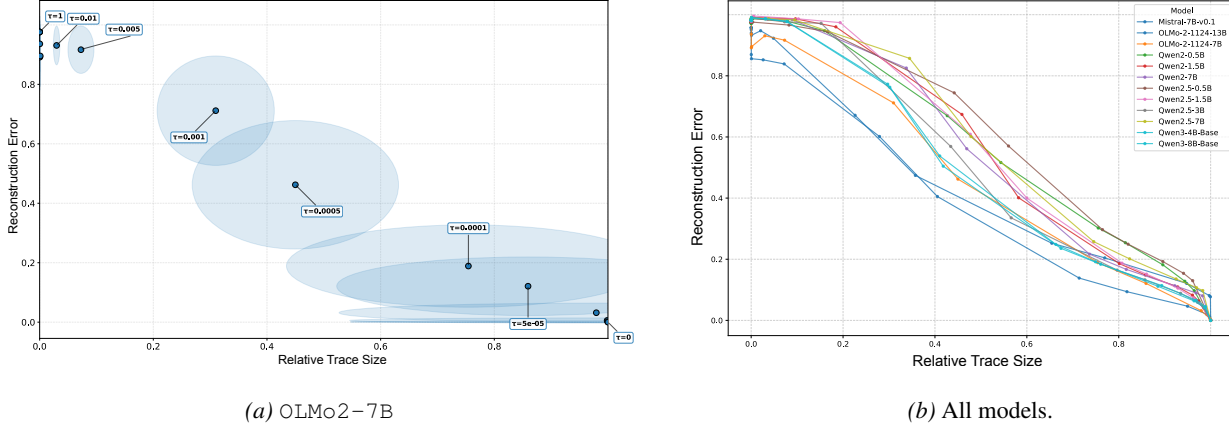


Figure 2. We extract the LLM’s trace at various threshold (τ), allowing to vary its granularity, and plot the relation between reconstruction error (measured with Total Variation distance) and trace size for various LLMs. On average, when τ is small (*bottom right corner*), the trace is large –consisting of almost the full model– and leads to a small reconstruction error. In contrast, when τ is large (*top left corner*), the trace is small –containing only few edges– and leads to a large reconstruction error. **Left (a), OLMo2-7B only:** Each ellipse in this graph represents one τ . Its is centered at the average size and reconstruction score of the resulting traces. Its horizontal and vertical diameters represent the variance (std) of the size and reconstruction score respectively. **Right (b), all models:** For the sake of readability, we only plot averages and omit the standard deviation.

size and the faithfulness of the trace, as previously defined. In a second step, combining the size and faithfulness at each threshold, we compute $\hat{\rho}$, our estimate of the density of the LLM when processing a given input.

We use 13 different base LLMs, from 5 families (Qwen[3, 2.5, 2](Yang et al., 2025),² OLMo 2 (OLMo et al., 2024) and Mistral V0.1 (Jiang et al., 2024a)), with sizes ranging in [0.5, 13] billion parameters, accessed through HuggingFace.

4.2. Results

We measure the extent to which the trace size influences its faithfulness. In other words, we look at how good the trace reconstruction is at various sizes, on average. If the computation within the LLMs is sparse, then a small trace should be able to faithfully reconstruct the full model distribution. A dense computation would result in a larger trace.

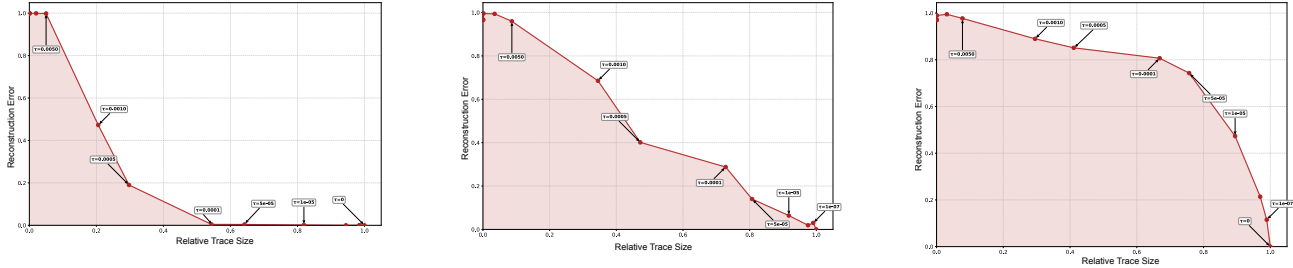
Trace Size vs. Faithfulness Let's first have a look at one model, namely OLMo2-7B. We represent the relation between size and faithfulness in Fig.2a. Each ellipse corresponds to a trace extracted at one threshold τ . Ellipses are centered at the mean trace size and mean reconstruction error, and the horizontal and vertical diameters represent the standard deviation of the size and error, respectively. We observe that the smallest trace (*top left corner*), while containing the most important edges, very poorly reconstructs the full model prediction. Reconstruction error decreases

approximately linearly with trace size, with no hint of a phase transition. To get a qualitative idea of what trace size captures, consider $\tau = 1e^{-3}$; OLMo2-7B's traces at this τ consist in 30% of the full model on average, and the trace is able to reconstruct a nucleus in $[0, 20]$ (see App. D). A nucleus reconstruction of 20 means that the trace recovers a distribution where the top-20% probability mass is equal to the one outputted by the full model. This is sufficient to produce at least the most likely token predicted by the full model. Finally, we reproduce the results with the other models in Fig. 2b (which omits standard deviations for clarity), finding that the pattern is universally shared.

Instance-level Density The mechanistic nature of the trace makes it possible to zoom in on individual instance. This enables looking at how the density varies across inputs. As an illustration, we plot in Fig. 3 the reconstruction error against the trace size for three inputs. These inputs were chosen to represent: (a) *low density*, where a near-perfect reconstruction is achieved with a small size; (b) *moderate density*, where the processing is neither sparse neither dense; and (c) *high density*, where almost the full model is required to get a small reconstruction error. The examples suggest that some input-dependent variability is present in terms of the portion of the computational graph required to process each input. This is supported by the data in Fig. 4, showing the distribution of density in our dataset for multiple LLMs, which is near-normal centered around middle values.

The fact that computation density is moderate on average, together with the previous results showing that reconstruc-

²Qwen's versions use distinct architectures and training data.



(a) **Low Density ($\bar{\rho} = 0.2$):** "In 1876, methylene blue was synthesized by German chemist Heinrich Caro. Paul Ehrlich in 1880 described the use"...

(b) **Moderate density** ($\hat{\rho} = 0.5$):
“Parish also found the music ‘downright painful’, which he contrasted with the ‘moody, atmospheric’”...

(c) **High Density** ($\hat{\rho} = 0.8$): “*The use of mathematics in the service of social and economic analysis dates back to the 17th century. Then*”...

Figure 3. We observed that the density varies across inputs, ranging from low (a) to high (c). We quantify this density by measuring the area under the curve when x is the relative trace size and y is the reconstruction error (TV Distance). Data obtained with OLMo2-7B.

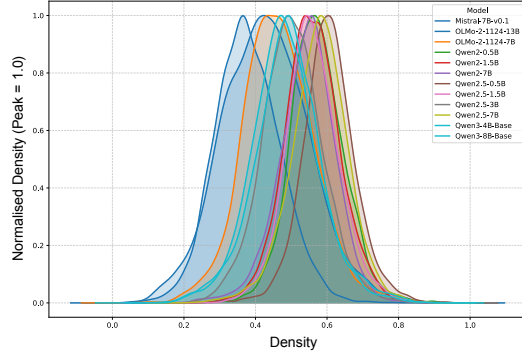


Figure 4. We plot the distribution of density for each model. We observe a significant variation of the density across inputs.

tion error falls linearly with trace size, calls into question the sparsity assumption underlying much of the mechanistic interpretability literature, especially the endeavor to identify *circuits*, or subgraphs in the network that are akin to algorithms learned by the LLM (Ferrando et al., 2024b). We provide empirical evidence that the assumption does not hold when using a more conservative faithfulness metric, which is important if we care about preserving good generation capability.

Fig. 4 also shows that there is a large variation across inputs. We next seek to understand the sources of this variation. We first check whether different models process the same inputs with comparable densities. If so, this would strongly suggest that density variation is indeed related to properties of the input, rather than to characteristics of the LLMs themselves. We measure the Spearman correlation of densities across LLMs and observe a rather substantial correlation between each pair (Fig. 5), with a mean of 0.48 (SD=0.09). This suggests that the variation in computation density is not only universal across LLMs, but also that certain input features

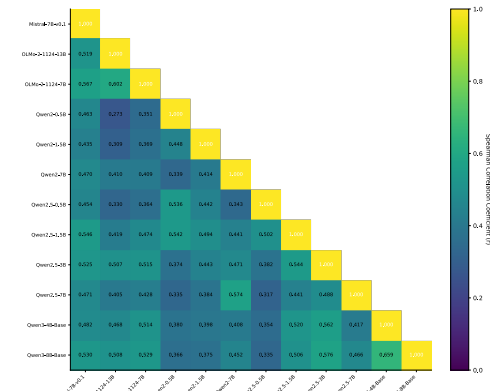


Figure 5. Spearman correlation of the density between pairs of LMs. In all cases, we observe a rather strong correlation.

trigger denser or sparser computation across all models.

Next, we measured the Pearson correlation between the entropy of the LLM’s output probability distribution and the instance-level density $\hat{\rho}$. This yields significant positive correlation across all models, of small magnitude, in the range $[0.06; 0.28]$ (full results in App. C.3). This means that traces tend to be larger when the model is less certain of the output, which we can tentatively take as an association between trace size and input complexity. However, the correlation is of small magnitude, and this test does not address the properties of the input itself, but the model’s response to it. The next experiment explores whether there is variation in density across inputs by analyzing input properties that are independent of the model.

5. Density Varies with Output Properties

While a broad range of lexical and syntactic properties can influence computational density, we focus on two features that provide clear, interpretable measures of distributional

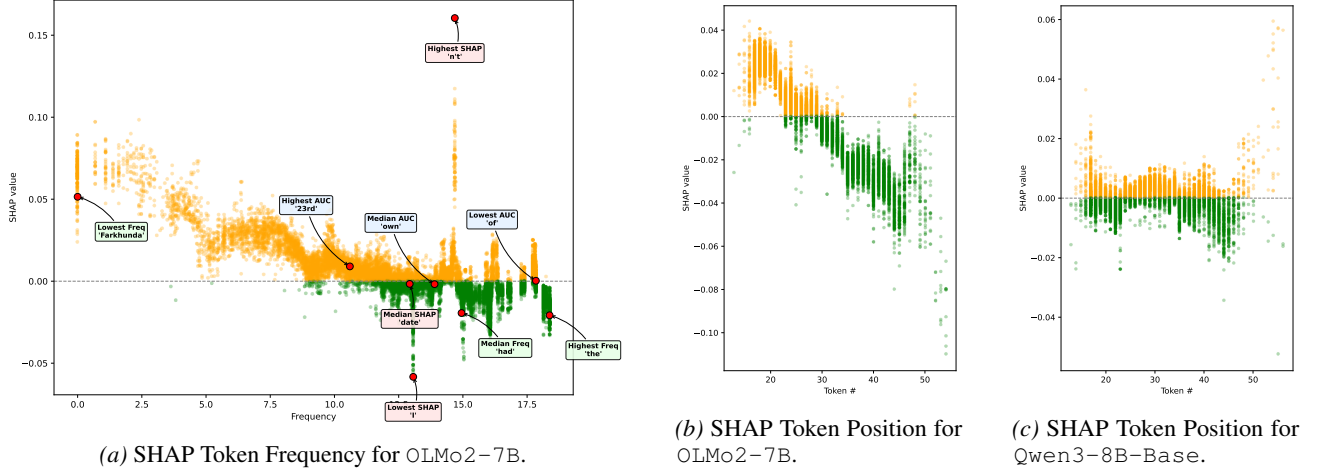


Figure 6. Feature analysis using SHAP values (a) Token Frequency: The relationship between token frequency and SHAP values indicates that rarer predictions involve denser computations. (b, c) Token Position: The impact of context size on model density. For some models, there is a clear trend where adding context (increasing token number) results in negative SHAP values, reducing density, while others are less sensitive to the context length.

and structural predictability: word frequency, and linear token position in the sequence. All else being equal, rarer words should be more difficult to predict (and thus require more computation); and planning the initial parts of a sentence should also be more difficult than the later parts, which are more deterministic given the beginning. We thus expect higher density for rarer words and earlier tokens, and the reverse for more frequent words and later tokens.

5.1. Method

In order to study how computational density depends on output properties, we collected a dataset of text *generated* by the LLM. To do so, we first curated a set of 660 prompts from diverse domains and corpora, with length ranging from 10 to 15 words (App. E). We used them to prompt the LLMs to generate 30-token continuations, using nucleus sampling with $p = 0.6$. For each generated token, we extract the trace at multiple levels of granularity, as done in Section 4, and we estimate the resulting density $\hat{\rho}$.

Although density is computed at the subword token level, we aggregate token-level values to full-word representations. Word-level aggregation reduces variance introduced by differences in tokenizer segmentation across models, enabling more interpretable and comparable analyses of prediction difficulty. For each word, we represent density as the maximum value among its constituent tokens, reflecting the peak uncertainty encountered during the generation of the word.

We then extract two properties: **Token # (Position)**, i.e. the word’s ordinal position relative to the start of the processed text (prompt + generated response), which also reflects the context size available to the model when making its prediction; and **Frequency**, calculated using a publicly available

token frequency list (see App. B). The analysis is done on the generated text only, excluding the prompts.

To quantify the impact of word properties on computation density, we employed a gradient-boosting regression approach using CatBoost model (Prokhorenkova et al., 2018). CatBoost is robust to heterogeneous feature types and captures nonlinear interactions automatically, while maintaining interpretability. In this model, computation density is the dependent variable, and Frequency and Token # the independent variables. For interpretation of the model, we utilized SHAP (SHapley Additive exPlanations) (Lundberg & Lee, 2017) values. SHAP assigns a value to each feature for each data point, representing that feature’s marginal contribution to the predicted density relative to the baseline. See App. B for more details. Positive SHAP values indicate that the feature increases the predicted density, while negative SHAP values indicate that the feature decreases the predicted density. This approach allows for comparing features’ importance relative to each other. We tested the same LLMs as in the first experiment, limited to the [7, 8] billion parameter range as to save computation resources.

5.2. Results

Assessing the features using the CatBoost+SHAP method largely gives support to our two predictions, as follows.

Rare predictions involve dense computations Fig. 6a shows the SHAP values for the frequency feature for OLMo2-7B, showing a pattern that we find in all models (see Fig. 12 in App. F). Recall that SHAP values indicate the magnitude and direction of the feature’s contribution to the predicted density. We observe that SHAP values increase as

tokens become rarer, indicating that low-frequency tokens are associated with higher density. Since low-frequency tokens can be expected to be harder to predict, this is another sign that the density of a computation may correlate with its difficulty for the model.

Adding more context often reduces density The effect of context size (measured in terms of Token Position) is less consistent. We find two patterns. For three of the models, the effect of this feature on density progressively goes down as token position increases, i.e. more context induces smaller computation density. In the other two, instead, we find a flatter pattern (see Fig. 6, and Fig. 13 in App. F). Interestingly, what we do find consistently is that the left-most data points, that correspond to the first tokens generated by the model after the prompt, are always associated to a positive (and often increasing) effect. We speculate that this could show the collusion of two trends: (1) increasing the context size reduces the density; (2) processing human-generated text (such as the prompt) increases the density as it is less “in-distribution” for the LLM than its own output.

6. Discussion

Our results suggest two primary conclusions: first, LLM computation is characterized by relatively high *density*; second, this density is strongly input-dependent. These findings have significant implications for three key areas of research.

Efficient pruning We find that while increasing computational sparsity is possible, it is strictly bounded. Consistent with Liu et al. (2023), we observe that achievable sparsity varies with the input. Crucially, however, aggressive pruning degrades the output probability distribution, often preserving only the mode (the top-1 token), while flattening the rest of the distribution. Relying on such truncated distributions is known to induce degenerate generation patterns, such as repetition loops (Holtzman et al., 2020). The current efficiency literature often relies on binary task-based metrics, which may obscure this degradation. We argue that pruning techniques must be evaluated against distributional metrics (like δ_{TV}) to ensure the preservation of generative quality.

Implications for Mechanistic Interpretability The observation of high computational density serves as a critical *caveat* for efforts to map LLM behaviors onto sparse circuits or discrete symbolic rules. We propose three recommendations for future circuit discovery work:

(1) *Adopt conservative metrics.* Circuit faithfulness should be evaluated on general language modeling (favor distribution preservation as much as possible) rather than simplified task metrics which can be satisfied by degenerated circuits.

(2) *Distinguish importance from sufficiency.* We demon-

strate that a subset of “most important” edges (by magnitude) is often not sufficient to reconstruct the output. Thus, attribution scores alone are not a proxy for sufficiency.

(3) *Account for redundancy.* The high density we observe might imply significant redundancy. A discovered “sparse circuit” may be just one of many redundant pathways capable of solving a task, rather than the unique mechanism.

On the positive side, mechanistic interpretability is a robust framework that need not be constrained to the search for sparse circuits. Integrating the computational graph formalism with broader *graph theory* offers a promising avenue for also analyzing dense, distributed processing. Our proposed density metric represents a first step in this direction. We hope this work encourages the community to explore other properties, such as *centrality* or *modularity*, to better characterize the complex internal dynamics of LLMs beyond simple circuit identification.

Implications for Cognitive Science The strong link between density and input variation, as well as the fact that density varies in similar ways across models, opens exciting avenues for research. Computational density could potentially serve as a novel metric for *linguistic complexity*. Moreover, our results suggest that LLMs recruit fewer resources for less demanding input (such as more frequent words), pointing to the idea that LLMs implement a form of *efficient processing*, in line with the emerging consensus on how humans process language (Gibson et al., 2019). Finally, studying which linguistic features trigger high or low density processing will inform how LLMs adapt resources to input difficulty, and when they use sparser versus denser processing, perhaps bridging the gap between symbolic and distributed views of language (Boleda, 2025).

Limitations Like all studies, ours has a number of limitations:

(a) Our computation density directly depends on how we identify the trace. Better methods could lead to smaller density, or emerging pattern we could not identify with the current approach.

(b) While we evaluate faithfulness through zero-ablation of the edges, recent work suggests that zero-ablation can move activations off the data manifold compared to mean-ablation or patching (Li & Janson, 2024). A more nuanced ablation, such as replacing with an edge with a mean edge vector, could provide a more accurate estimation of the trace faithfulness.

(c) Our study is limited to English data and the transformer architecture. Adapting it to other languages and architectures will be essential for tearing apart the effect of the input and the architecture.

Impact Statement

This work advances the field of Mechanistic Interpretability, which aims to elucidate the internal decision-making processes of Large Language Models (LLMs). By characterizing the limits of computational sparsity and proposing more rigorous faithfulness metrics, our research contributes to the development of more transparent and accountable AI systems. Understanding the true density of information flow is a prerequisite for reliable model monitoring, debugging, and safety auditing.

We do not foresee any direct negative societal impacts from this work. While insights into model efficiency could theoretically be used to optimize harmful systems, the primary application of our findings is to prevent oversimplified explanations of model behavior, thereby fostering more robust safety evaluations.

References

Ameisen, E., Lindsey, J., Pearce, A., Gurnee, W., Turner, N. L., Chen, B., Citro, C., Abrahams, D., Carter, S., Hosmer, B., Marcus, J., Sklar, M., Templeton, A., Bricken, T., McDougall, C., Cunningham, H., Henighan, T., Jermyn, A., Jones, A., Persic, A., Qi, Z., Ben Thompson, T., Zimmerman, S., Rivoire, K., Conerly, T., Olah, C., and Batson, J. Circuit tracing: Revealing computational graphs in language models. *Transformer Circuits Thread*, 2025. URL <https://transformer-circuits.pub/2025/attribution-graphs/methods.html>.

Bansal, H., Gopalakrishnan, K., Dingliwal, S., Bodapati, S., Kirchhoff, K., and Roth, D. Rethinking the role of scale for in-context learning: An interpretability-based case study at 66 billion scale. In *Proceedings of the 61st Annual Meeting of the Association for Computational Linguistics (Volume 1: Long Papers)*, pp. 11833–11856, 2023.

Bhaskar, A., Wettig, A., Friedman, D., and Chen, D. Finding transformer circuits with edge pruning. *Advances in Neural Information Processing Systems*, 37:18506–18534, 2024.

Boleda, G. LLMs as a synthesis between symbolic and distributed approaches to language. In *Findings of the ACL: EMNLP 2025*, pp. 9365–9379, 2025. URL <https://aclanthology.org/2025.findings-emnlp.498/>.

Bricken, T., Templeton, A., Batson, J., Chen, B., Jermyn, A., Conerly, T., Turner, N., Anil, C., Denison, C., Askell, A., Lasenby, R., Wu, Y., Kravec, S., Schiefer, N., Maxwell, T., Joseph, N., Hatfield-Dodds, Z., Tamkin, A., Nguyen, K., McLean, B., Burke, J. E., Hume, T., Carter, S., Henighan, T., and Olah, C. Towards monosemanticity: Decomposing language models with dictionary learning. *Transformer Circuits Thread*, 2023. <https://transformer-circuits.pub/2023/monosemantic-features/index.html>.

Cammarata, N., Carter, S., Goh, G., Olah, C., Petrov, M., Schubert, L., Voss, C., Egan, B., and Lim, S. K. Thread: Circuits. *Distill*, 2020. doi: 10.23915/distill.00024. <https://distill.pub/2020/circuits>.

Conmy, A., Mavor-Parker, A., Lynch, A., Heimersheim, S., and Garriga-Alonso, A. Towards automated circuit discovery for mechanistic interpretability. In *Proceedings of NeurIPS*, volume 36, pp. 16318–16352, New Orleans, LA, 2023.

Elhage, N., Nanda, N., Olsson, C., Henighan, T., Joseph, N., Mann, B., Askell, A., Bai, Y., Chen, A., Conerly, T., et al. A mathematical framework for transformer circuits. *Transformer Circuits Thread*, 2021.

Fan, S., Jiang, X., Li, X., Meng, X., Han, P., Shang, S., Sun, A., Wang, Y., and Wang, Z. Not all layers of llms are necessary during inference. *arXiv preprint arXiv:2403.02181*, 2024.

Ferrando, J. and Voita, E. Information flow routes: Automatically interpreting language models at scale. In *Proceedings of the 2024 Conference on Empirical Methods in Natural Language Processing*, 2024.

Ferrando, J., Sarti, G., Bisazza, A., and Costa-jussá, M. A primer on the inner workings of transformer-based language models. <https://arxiv.org/abs/2405.00208>, 2024a.

Ferrando, J., Sarti, G., Bisazza, A., and Costa-Jussà, M. R. A primer on the inner workings of transformer-based language models. *arXiv preprint arXiv:2405.00208*, 2024b.

Frankle, J. and Carbin, M. The lottery ticket hypothesis: Finding sparse, trainable neural networks. In *Proceedings of ICLR*, New Orleans, LA, 2019. Published online: <https://openreview.net/group?id=ICLR.cc/2019/conference>.

Gibson, E., Piantadosi, R. F. S., Dautriche, I., Mahowald, K., Bergen, L., and Levy, R. How efficiency shapes human language. *Trends in Cognitive Science*, 23(5):389–407, 2019.

Hanna, M., Liu, O., and Variengien, A. How does gpt-2 compute greater-than?: Interpreting mathematical abilities in a pre-trained language model. *Advances in Neural Information Processing Systems*, 36:76033–76060, 2023.

Hanna, M., Pezzelle, S., and Belinkov, Y. Have faith in faithfulness: Going beyond circuit overlap when finding model mechanisms. *arXiv preprint arXiv:2403.17806*, 2024.

Holtzman, A., Buys, J., Du, L., Forbes, M., and Choi, Y. The curious case of neural text degeneration. In *International Conference on Learning Representations*, 2020. URL <https://openreview.net/forum?id=rygGQyrFvH>.

Jackendoff, R. and Wittenberg, E. What you can say without syntax: A hierarchy of grammatical complexity. In Newmeyer, F. and Preston, L. (eds.), *Measuring Grammatical Complexity*, pp. 65–82. Oxford University Press, Oxford, UK, 2014.

Jiang, A. Q., Sablayrolles, A., Mensch, A., Bamford, C., Chaplot, D. S., Casas, D., et al. Mistral 7b. *arXiv preprint arXiv:2310.06825*, 2024a.

Jiang, Y., Wang, H., Xie, L., Zhao, H., Qian, H., Lui, J., et al. D-llm: A token adaptive computing resource allocation strategy for large language models. *Advances in Neural Information Processing Systems*, 37:1725–1749, 2024b.

Lad, V., Lee, J. H., Gurnee, W., and Tegmark, M. The remarkable robustness of llms: Stages of inference? *arXiv preprint arXiv:2406.19384*, 2024.

LeCun, Y., Denker, J., and Solla, S. Optimal brain damage. *Advances in neural information processing systems*, 2, 1989.

Lee, A., Che, E., and Peng, T. How well do llms compress their own chain-of-thought? a token complexity approach. *arXiv preprint arXiv:2503.01141*, 2025.

Lee, D., Lee, J.-Y., Zhang, G., Tiwari, M., and Mirhoseini, A. Cats: Contextually-aware thresholding for sparsity in large language models. *arXiv preprint arXiv:2404.08763*, 2024.

Li, M. and Janson, L. Optimal ablation for interpretability. *Advances in Neural Information Processing Systems*, 37:109233–109282, 2024.

Li, W., Li, L., Lee, M., and Sun, S. Adaptive layer sparsity for large language models via activation correlation assessment. *Advances in Neural Information Processing Systems*, 37:109350–109380, 2024.

Liu, Z., Wang, J., Dao, T., Zhou, T., Yuan, B., Song, Z., Shrivastava, A., Zhang, C., Tian, Y., Re, C., et al. Deja vu: Contextual sparsity for efficient llms at inference time. In *International Conference on Machine Learning*, pp. 22137–22176. PMLR, 2023.

Lundberg, S. M. and Lee, S.-I. A unified approach to interpreting model predictions. *Advances in neural information processing systems*, 30, 2017.

Luo, Y., Song, C., Han, X., Chen, Y., Xiao, C., Meng, X., Deng, L., Wei, J., Liu, Z., and Sun, M. Sparsing law: Towards large language models with greater activation sparsity. *arXiv preprint arXiv:2411.02335*, 2024.

Méloux, M., Maniu, S., Portet, F., and Peyrard, M. Everything, everywhere, all at once: Is mechanistic interpretability identifiable? In *The Thirteenth International Conference on Learning Representations*, 2025.

Meng, K., Bau, D., Andonian, A., and Belinkov, Y. Locating and editing factual associations in gpt. In *Advances in Neural Information Processing Systems*, volume 35, pp. 17359–17372, 2022.

Merity, S., Xiong, C., Bradbury, J., and Socher, R. Pointer sentinel mixture models. In *Proceedings of ICLR Conference Track*, Toulon, France, 2017. Published online: <https://openreview.net/group?id=ICLR.cc/2017/conference>.

Michel, P., Levy, O., and Neubig, G. Are sixteen heads really better than one? *Advances in neural information processing systems*, 32, 2019.

Olah, C., Satyanarayan, A., Johnson, I., Carter, S., Schubert, L., Ye, K., and Mordvintsev, A. The building blocks of interpretability. *Distill*, 2018.

OLMo, T., Walsh, P., Soldaini, L., Groeneveld, D., Lo, K., Arora, S., et al. 2 olmo 2 furious. *arXiv preprint arXiv:2501.00656*, 2024.

Prokhorenkova, L., Gusev, G., Vorobev, A., Dorogush, A. V., and Gulin, A. Catboost: unbiased boosting with categorical features. *Advances in neural information processing systems*, 31, 2018.

See, A., Liu, P. J., and Manning, C. D. Get to the point: Summarization with pointer-generator networks. In *Proceedings of the 55th Annual Meeting of the Association for Computational Linguistics (Volume 1: Long Papers)*, pp. 1073–1083, Vancouver, Canada, July 2017. Association for Computational Linguistics. doi: 10.18653/v1/P17-1099. URL <https://www.aclweb.org/anthology/P17-1099>.

Sharkey, L., Chughtai, B., Batson, J., Lindsey, J., Wu, J., Bushnaq, L., Goldowsky-Dill, N., Heimersheim, S., Ortega, A., Bloom, J., et al. Open problems in mechanistic interpretability. *arXiv preprint arXiv:2501.16496*, 2025.

Smolensky, P., McCoy, R., Fernandez, R., Goldrick, M., and Gao, J. Neurocompositionality: From the central paradox of cognition to a new generation of ai systems. *AI Magazine*, 43(3):308–322, 2022.

Sun, M., Liu, Z., Bair, A., and Kolter, J. Z. A simple and effective pruning approach for large language models. *arXiv preprint arXiv:2306.11695*, 2023.

Syed, A., Rager, C., and Conmy, A. Attribution patching outperforms automated circuit discovery. In *Proceedings of the 7th BlackboxNLP Workshop: Analyzing and Interpreting Neural Networks for NLP*, pp. 407–416, 2024.

Vaswani, A., Shazeer, N., Parmar, N., Uszkoreit, J., Jones, L., Gomez, A. N., Kaiser, Ł., and Polosukhin, I. Attention is all you need. In *Advances in Neural Information Processing Systems*, volume 30, 2017.

Voita, E., Ferrando, J., and Nalmpantis, C. Neurons in large language models: Dead, n-gram, positional. <https://arxiv.org/abs/2309.04827>, 2023.

Wang, K., Variengien, A., Conmy, A., Shlegeris, B., and Steinhardt, J. Interpretability in the wild: a circuit for indirect object identification in gpt-2 small. *arXiv preprint arXiv:2211.00593*, 2022.

Yang, A., Li, B., Yang, B., Zhang, B., Hui, B., Zheng, B., et al. Qwen3 technical report. *arXiv preprint arXiv:2505.09388*, 2025.

Zhang, Z., Lin, Y., Liu, Z., Li, P., Sun, M., and Zhou, J. Moefication: Transformer feed-forward layers are mixtures of experts. In *Findings of the Association for Computational Linguistics: ACL 2022*, pp. 877–890, 2022.

Zhu, Y., Kiros, R., Zemel, R., Salakhutdinov, R., Urtasun, R., Torralba, A., and Fidler, S. Aligning books and movies: Towards story-like visual explanations by watching movies and reading books. In *Proceedings of ICCV*, pp. 19–27, Santiago, Chile, 2015.

A. Code and Resources

We developed the code for extracting and evaluating the trace from Hugging Face models. We leverage Pytorch *hooks* in order to extract LLM’s internal representations when constructing the computational graph, as well as to ablate edges during the ablation. The code and data required to reproduce the experiments will be made publicly available on a Github repository upon acceptance.

B. Method: Additional Information (from Section 3)

Threshold Values For Trace Extraction In order to extract the trace at different size, we empirically set $\tau \in [1e-7, 1e-6, 1e-5, 5e-5, 1e-4, 5e-4, 1e-3, 5e-3, 1e-2, 5e-2, 0.1, 0.2, 0.4, 0.8, 1.0]$, as we found these span diverse trace size ranging from sparse to dense. These values were obtained after manually testing the resulting trace size on few instances.

CatBoost Setup To ensure our findings were not artifacts of a specific data split, we implemented a cross-validation strategy. Instead of a single training run, the modeling pipeline was executed 10 times. In each iteration, the dataset was randomly reshuffled and split into training (70%) and testing (30%) sets using a unique random seed. Results were aggregated across the 10 runs to produce robust estimates.

Tokenization and Frequency in Section 5 In Section 5 we use “token” rather than “word” because we include punctuation and other symbols. More precisely, we rely on spaCy tokens (<https://spacy.io/>). We take frequency estimates from the ukWaC unigrams list available at https://wacky.sslmit.unibo.it/doku.php?id=frequency_lists.

C. Additional Results

C.1. Random trace extraction baseline

As a sanity check, we compare our trace extraction method to a random one. To do so, for each trace T with size s extracted using the method introduced in Section 3, we randomly extract a subgraph R of size s . We make sure that this subgraph is connected. By default, the residual edges are always included in the random graph. We indeed observed that ablating the residual edges lead to very weak random baseline, therefore, we decided to never ablate residual edges in the random graph. We use a subset of the dataset used in Section 4, comprising 1000 instances, and tested the OLMo2-7B model. Results are shown in Fig. 8. We observe that the trace extraction method used in this paper outperforms the random baseline at any size (at equivalent reconstruction score, our method leads to a smaller trace in average).

C.2. Sufficient vs. Necessary

As a second sanity check, we measure the effect of ablating the trace size only. In that setup, we zeroed the edges in the computational graph that belongs to the trace (instead on keeping only the edges that belong to the graph). We use a subset of the dataset used in Section 4, comprising 1000 instances, and tested the OLMo2-7B model. Results are shown in Fig. 9. In this setup, we never ablate the edges residual (neither for our trace extraction nor the random baseline), as it would automatically and significantly degrade the output probability. We observe that the edges identified by our trace extraction method are indeed necessary to reconstruct a faithful output. Here again, the trace extraction we used in the paper outperforms the random baseline.

C.3. Density vs. Entropy

Fig. 7 shows the correlation between density and the entropy of the LLM output.

D. Nucleus Reconstruction

An alternative reconstruction measure (more interpretable, but less stable than the total variation distance) is the size of the largest nucleus that can be reconstructed by the trace. For instance, a score of 20 tells us that the trace recovers a distribution where the top-20% probability mass is equal to the one outputted by the full model. Fig. 10 shows this alternative metric for OLMo2-7B.

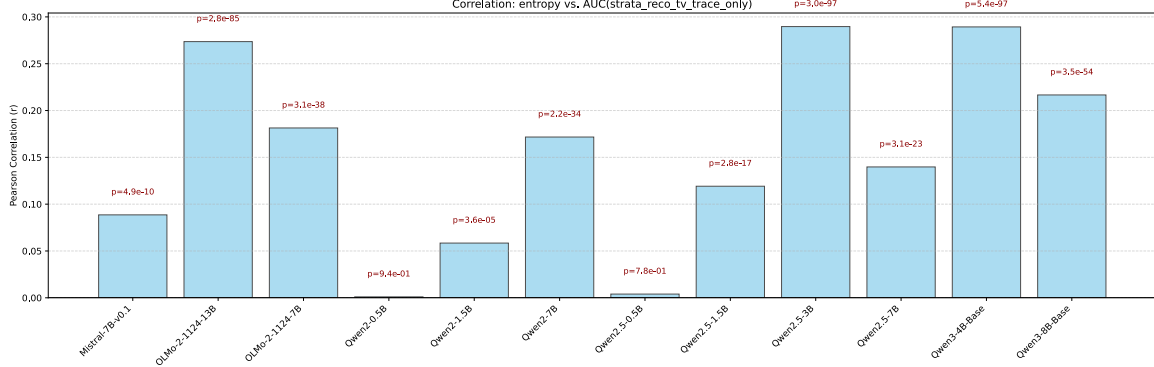


Figure 7. Pearson correlation between computation density and the entropy of the output probability distribution.

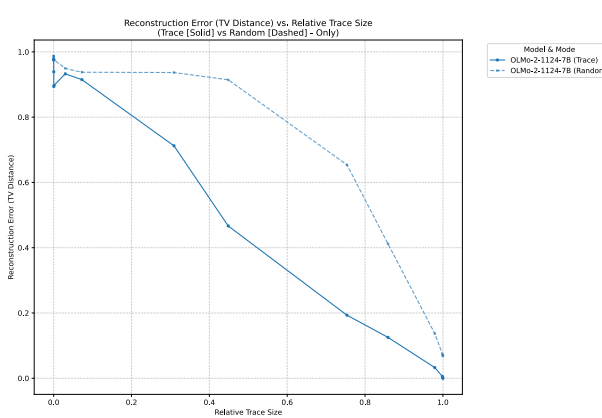


Figure 8. We compare our trace extraction with a random baseline. The trace extraction method used in this paper outperforms the random baseline at any size. Model = OLMo2-7B

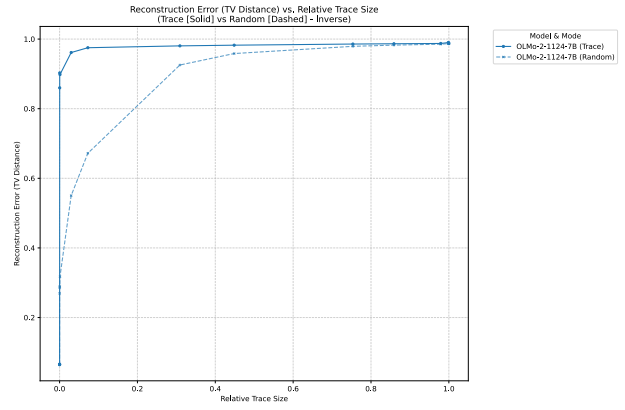


Figure 9. We measure how necessary is the trace for a faithful reconstruction, by ablating only the edges that belongs to the trace. We observe that the edges identified by our trace extraction method are indeed necessary. In addition, it outperforms the random baseline. Model = OLMo2-7B

E. Prompt Dataset of Section 5

The dataset targets three distinct domains representing literary, journalistic, and encyclopedic registers.

Data Sources Input data was streamed from three diverse corpora to ensure stylistic and topical variance:

- **Literary:** *BookCorpus* (Zhu et al., 2015), representing narrative fiction.
- **Journalistic:** *CNN/DailyMail* (See et al., 2017), representing news summaries and articles.
- **Encyclopedic:** *Wikitext-103* (Merity et al., 2017), representing curated informational text.

Documents were segmented into sentences using the Spacy English pipeline (en_core_web_sm). To ensure meaningful context, we enforced a prompt length constraint of L tokens, where $15 \leq L \leq 25$. The mining process was designed to balance the distribution of the final token in the prompt across specific grammatical categories. We targeted 11 distinct Part-of-Speech (POS) categories to ensure broad syntactic coverage: *Noun, Proper Noun, Verb, Adjective, Adverb, Pronoun, Determiner, Auxiliary, Punctuation*, as well as grouped functional categories (*ADP+PART* and *CCONJ+SCONJ*).

To ensure the prompts were naturalistic, grammatically correct, and solvable without external context, several filtering heuristics were applied:

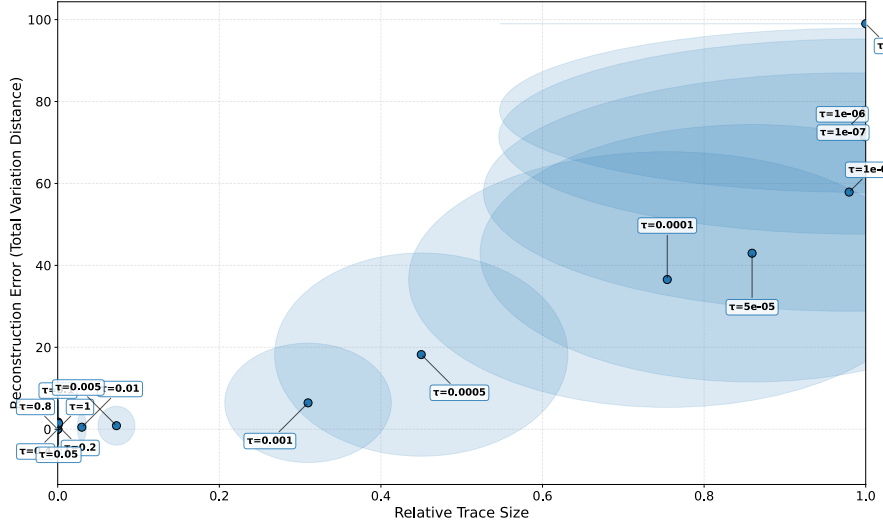


Figure 10. Nucleus Reconstruction (higher is better)

Figure 11. We extract the LLM’s trace at various threshold (τ), allowing to vary its granularity. Each ellipse in this graph represents one τ . Its is centered at the average size and nucleus reconstruction score of the resulting traces. Its horizontal and vertical diameters represent the variance (std) of the size and reconstruction score respectively. The Nucleus Reconstruction score tells us what is the largest nucleus a trace is able to reconstruct. Model = OLMO2-7B

- **Sentence Initiation:** Candidates were rejected if they began with punctuation marks or coordinating conjunctions (e.g., *And, But*), which typically indicate fragmentary context. We enforced strict capitalization for the News and Wiki domains, while relaxing this constraint for *BookCorpus* to accommodate its native lowercase formatting.
- **Artifact Removal:** We implemented a regular-expression based detokenization layer to correct pre-processing artifacts common in the source corpora. This included normalizing Moses-style double quotes (e.g., `"word"` \rightarrow `word`), correcting spacing around parentheses and punctuation, and resolving split contractions (e.g., `did n't` \rightarrow `didn't`).
- **Self-Contained Constraint:** To eliminate ambiguous anaphora, we enforced a strict resolution rule for third-person pronouns. Prompts containing pronouns (*he, she, it, they*) or demonstratives (*this, that*) were rejected unless a valid antecedent (a Proper Noun or Noun) was detected within the preceding four tokens.

To maximize topic diversity and prevent data clustering (e.g., extracting multiple prompts from a single book or article), we implemented a stochastic skipping mechanism. Upon successfully extracting a valid prompt, the pipeline discards a random interval of subsequent documents ($10 \leq N \leq 50$) before resuming the search. This ensures that the resulting dataset represents a broad cross-section of the underlying corpora.

F. Additional SHAP results

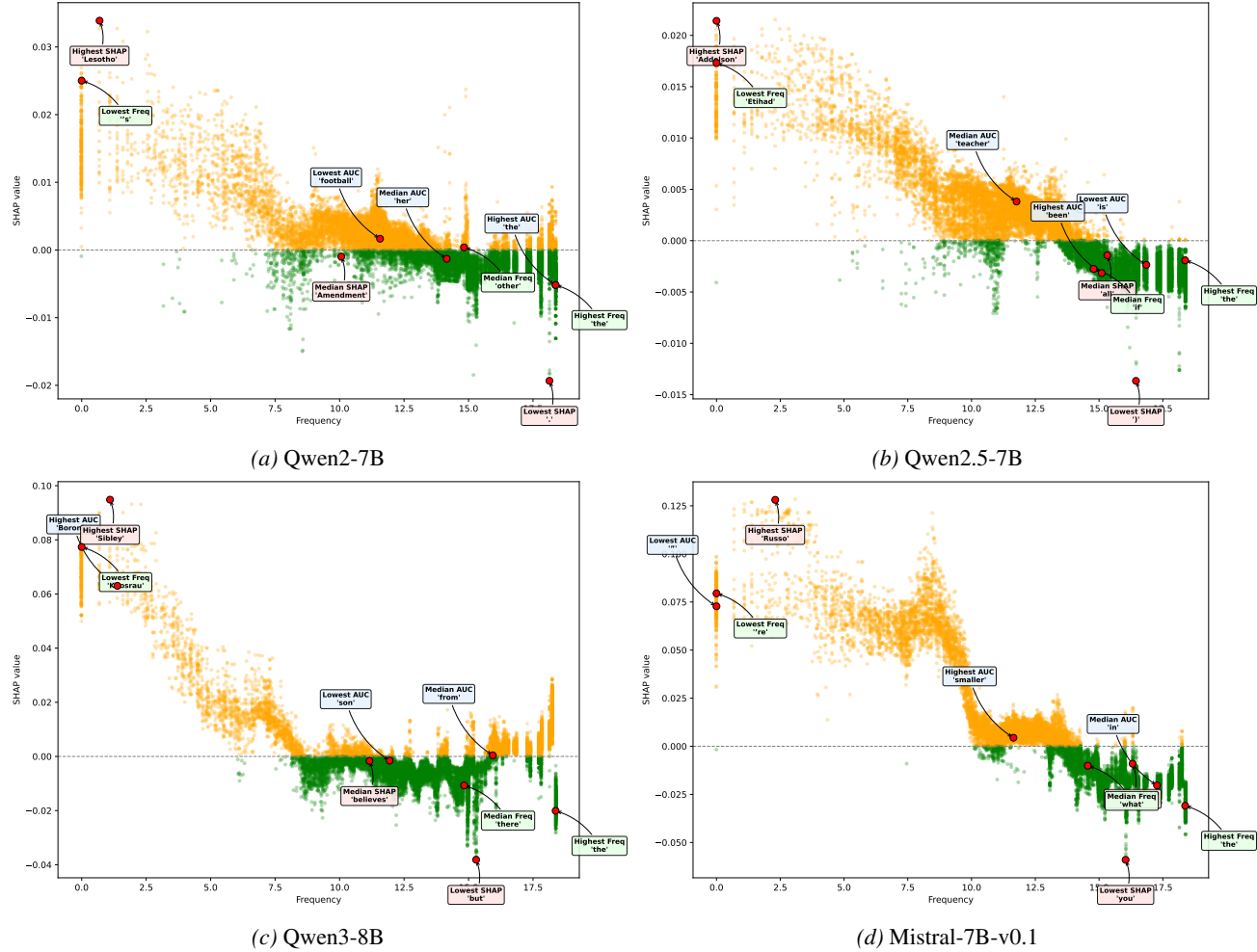


Figure 12. Frequency vs. SHAP values

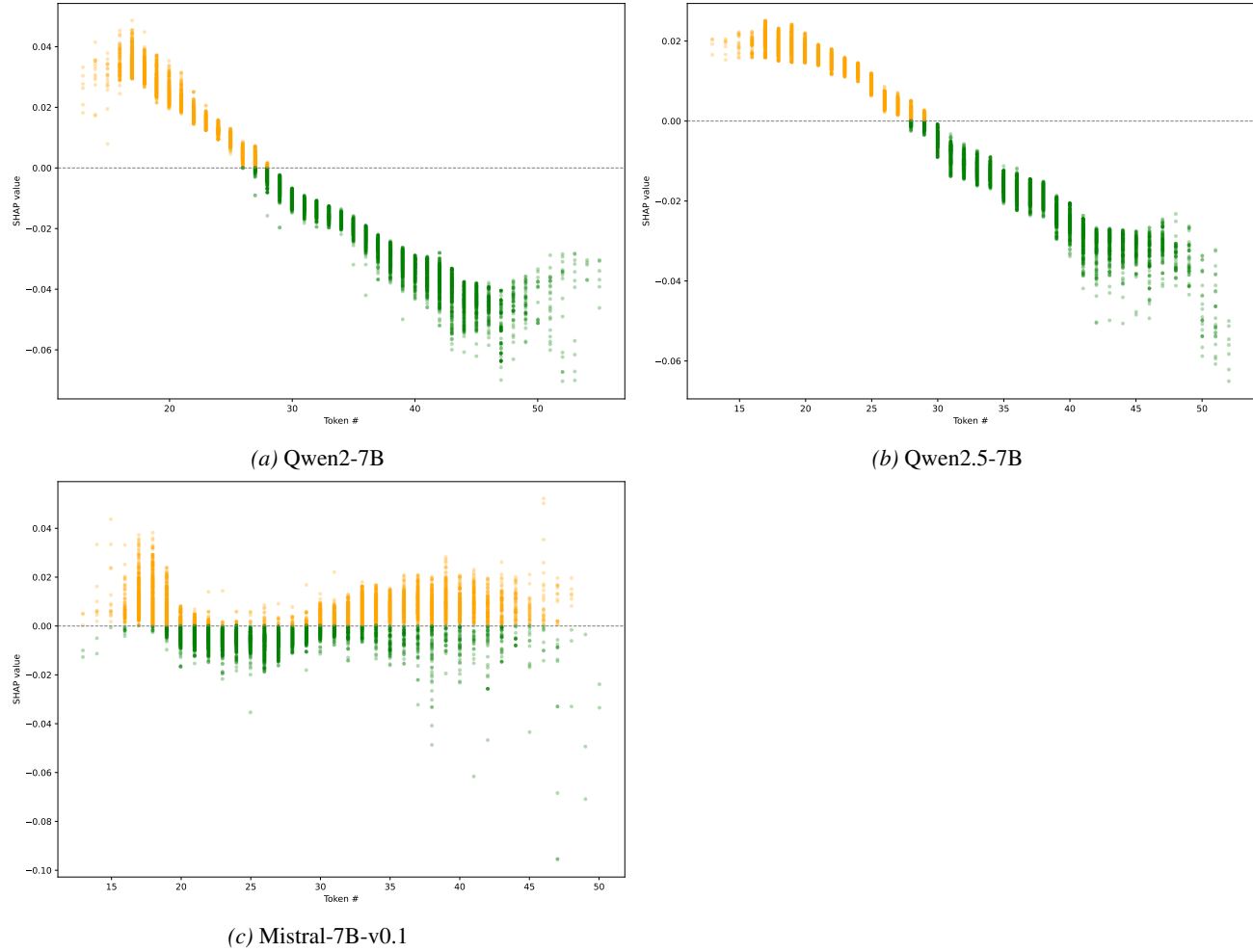


Figure 13. Position vs. SHAP values